ACS APPLIED MATERIALS & INTERFACES

RESEARCH ARTICLE

www.acsami.org

Mechanisms of Combustion Synthesis and Magnetic Response of High-Surface-Area Hexaboride Compounds

Raghunath Kanakala,[†] Roberto Escudero,[‡] Gabriel Rojas-George,[§] Mohan Ramisetty,[†] and Olivia A. Graeve[†,*]

[†]Kazuo Inamori School of Engineering, Alfred University, 2 Pine Street, Alfred, New York 14802, United States

[‡]Instituto de Investigaciones en Materiales, Universidad Nacional Autónoma de México, Apartado Postal 70-360 México, D.F. 04510

[§]Department of Chemical and Metallurgical Engineering, University of Nevada, Reno, 1664 N. Virginia Street, MS 388, Reno, Nevada 89557, United States

ABSTRACT: We present an analysis of the combustion synthesis mechanisms for the preparation of hexaboride materials using three compounds as model systems: EuB_6, YbB_6, and YB_6. These three hexaborides were chosen because of the differences in ionic radii between Eu^{3+}, Yb^{3+}, and Y^{3+}, which is a factor in their stability. The powders were prepared using metal nitrates, carbohydrazide, and two different boron precursor powders. The resulting materials were analyzed by X-ray diffraction, which showed that combustion synthesis is effective for the synthesis of EuB_6, since the Eu^{3+} ion has an ionic radius greater than ~1 Å. The synthesis of YbB_6 and YB_6 is not as effective because of the small size of the Yb^{3+} and Y^{3+} ions, making the hexaborides of these metals less stable and resulting in the synthesis of borates due to the presence of oxygen during the combustion process. Scanning electron microscopy and dynamic light scattering of the EuB_6 powders shows that the particle size of the hexaboride product is dependent on the particle size of the boron precursor. The magnetic susceptibility of our EuB_6 powders manifests irreversible behavior at low applied fields, which disappears at higher fields. This behavior can be attributed to the increase in size and number of magnetic polarons with increasing magnetic field.

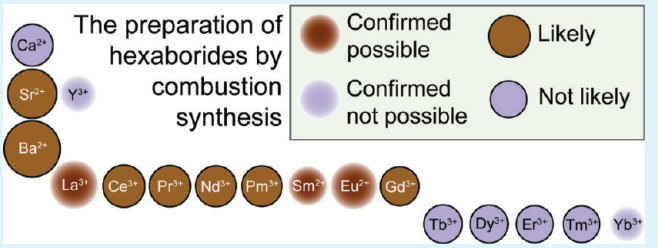

KEYWORDS: hexaboride, combustion synthesis, boron, particle size, magnetic susceptibility, nanopowders

1. INTRODUCTION

Rare earth and alkaline earth hexaborides have potential uses in a variety of engineering applications because of their unique electrochemical and magnetic properties. These properties stem from their singular crystal structure. The lattice is simple cubic with boron octahedra at each corner of the cube bonded at the apexes. The octahedra consist of boron atoms, with four adjacent neighbors in every octahedron for every boron atom and one on the main axes of the cube. The boron valence electrons are distributed over five bonds. The metal atom is located in the middle of the unit cell and can donate electrons to the structure, imparting a metallic character to hexaborides with metal ions of +3 charge, and semiconductor character to hexaborides with metal ions of +2 charge. This, together with the strong bonds between the boron atoms in the framework, produces a series of compounds that have high thermal and chemical stabilities.

In addition, these compounds have long been studied as model materials in solid state physics because of their intriguing variations in electrical, magnetic, and thermal properties. EuB_6, for example, is poorly conducting in its higher temperature paramagnetic state, but exhibits anomalous and unique electrical and magnetic transitions at low temperatures. A temperature of about 15 K marks the appearance of a weak magnetic moment. At about 12 K a second transition is observed, associated with the bulk Curie temperature and the transformation to a ferromagnetic state. It has been postulated that the higher temperature transition is due to metallization via the overlap and coalescence of magnetic polarons,[1−6] which can increase in size by lowering the temperature or increasing the magnetic field. These magnetic polarons are composite entities of localized charge carriers with aligned spins in a background of local moments. At this transition, EuB_6 is separated into two magnetic phases, one conducting and ferromagnetically ordered and the other poorly conducting and paramagnetic. The ferromagnetic phase only affects approximately 15% of the europium 4f electron moments. As the temperature decreases, the fraction of the ferromagnetic phase is increased until the material becomes a bulk ferromagnet. The presence of the ferromagnetic phase in this material can be accounted for by a lowering of the lattice symmetry from the cubic Pm3m space group of this structure to one of the tetragonal subgroups, or possibly a lower orthorhombic phase, resulting from the formation of a noncubic environment in the B_6 octahedra of the crystal.[7,8]

Rhyee and Cho[9] have found magnetic irreversibility for single crystals of $Eu_{0.9}La_{0.1}B_6$ at fields of 100 Oe and attributed it to the presence of the La dopant, which causes significant magnetic frustration and plays a role in the formation of magnetic polarons,[10]

Received: December 13, 2010
Accepted: March 26, 2011
Published: March 26, 2011

leading to a magnetically unstable state at low fields. Wigger et al.[11] have found that if single crystals of EuB_6 are doped with Ca^{2+} ($Ca_{1-x}Eu_xB_6$), the Curie temperature decreases substantially with increasing amounts of Ca^{2+}. When the dopant reaches a critical value of about $x \geq 0.3$, the Curie temperature is completely suppressed and the material no longer exhibits ferromagnetism. Snow et al.[6] similarly have found that for La^{3+}-doped EuB_6 ($Eu_{1-y}La_yB_6$) single crystals, the magnetic susceptibility and the Curie temperature decrease with increasing amounts of La^{3+}. Their results show that small amounts of dopants ($y \leq 0.01$) have little effect on magnetic behavior, attributable to the highly local and pure-spin nature of the polarons. However, at $y \geq 0.03$ no magnetic polarons are present eliminating all magnetic response from the material.

On the basis of our earlier study on the synthesis of LaB_6 and SmB_6,[12] we now present further evidence on the mechanisms of solution combustion synthesis for the preparation of three hexaborides, EuB_6, YbB_6, and YB_6, and a detailed analysis of product characteristics and magnetic behavior of EuB_6. These hexaborides were chosen as model systems for analysis of the chemistry of the combustion process because of the differences in ionic radii between Eu^{3+}, Yb^{3+}, and Y^{3+}, which is a factor in their stability.

2. EXPERIMENTAL PROCEDURE

The reactants for the synthesis of the hexaborides were $Eu(NO_3)_3 \cdot 6H_2O$ (99.99%, Alfa Aesar, Ward Hill, MA), $Y(NO_3)_3 \cdot 6H_2O$ (99.99%, Alfa Aesar, Ward Hill, MA), $Yb(NO_3)_3 \cdot 6H_2O$ (99.99%, Alfa Aesar, Ward Hill, MA), carbohydrazide (CH_6N_4O, 98%, Sigma-Aldrich, St. Louis, MO), boron (B1) powders (98%, Sigma-Aldrich, St. Louis, MO), and boron (B2) powders (Noval Industrial Group, Shandong, China). A typical reaction consisted of 10.2865 g of $Eu(NO_3)_3 \cdot 6H_2O$, 1.4957 g of boron, and 0.5193 g of carbohydrazide, for the case of EuB_6 synthesis, 12.4547 g of $Y(NO_3)_3 \cdot 6H_2O$, 2.1091 g of boron, and 1.4647 g of carbohydrazide, for the case of YB_6 synthesis, and 9.4395 g of $Yb(NO_3)_3 \cdot 6H_2O$, 1.3632 g of boron, and 0.9467 g of carbohydrazide, for the case of YbB_6 synthesis. The fuel-to-oxidizer ratio for all experiments was maintained at 0.083, which is very fuel lean and resulting in combustion temperatures below 1000 °C. The details of the synthesis procedure and cleaning techniques are provided in ref 12. In brief, the synthesis was completed by placing the reactants in a muffle furnace and heating to 593 K using a heating rate of ~20 °C/min. The washing process involved a series of steps: (1) cleaning with 80 mL of HCl and 20 mL of H_2O for every 1 g of the powder, and centrifuging at 4000 rpm for 30 min, (2) washing with 100 mL of deionized water and centrifuging, (3) cleaning with 50 mL of H_2SO_4 and 50 mL of H_2O for every 1 g of the powder, followed by centrifuging, (4) washing with deionized water and centrifuging, and (5) air drying. We employed diluted hydrochloric acid (12.1 M, Fisher Scientific, Pittsburgh, PA 15275) and diluted sulfuric acid (18 M, Fisher Scientific, Pittsburgh, PA 15275).

Characterization of the powders was carried out by X-ray diffraction (XRD) on a Philips PW 1800 system (Koningklÿke Philips Electronics N.V., Eindhoven, The Netherlands). For XRD, the powders were ground by hand using a mortar and pestle, and then spread evenly on the surface of the sample holder. The powders were lightly tapped to form a smooth surface. The experiment was run using CuKα radiation. Scanning electron microscopy (SEM) of the powders was completed on a FEI Quanta 200F system (FEI Company, Hillsboro, OR) with an AMETEK Sapphire Si(Li) EDS detector. The samples were prepared by dispersing the powders in acetone and drop-coating on a silicon wafer. Samples were also prepared for energy-dispersive spectroscopy by embedding the powders in epoxy and polishing across to expose the internal volume of the powders.

X-ray photoelectron spectroscopy (XPS) was completed on a PHI Quantera SXM system (Physical Electronics, Inc., Chanhassen, MN). The spectra were obtained using monochromated Al Kα radiation with energy of 1486.6 eV. A 200 μm/15 kV/26 eV pass energy beam was used for all analyses and the pressure was kept at 1×10^{-9} Torr. Sputter depth profiling was performed for XPS analysis on samples using a 3 kV power setting for 2 min over a 3 by 3 mm raster area. Analyses were undertaken using single pass survey scans over a range of 0 to 1300 eV using a pass energy of 224 eV. Surface charging effects were corrected with the C 1s peak at 284.6 eV as a reference. The XPS signals were analyzed by using a peak synthesis program in which a nonlinear background was assumed and the fitting peaks of the experimental curve were defined by Gaussian−Lorentzian distributions. X-ray fluorescence (XRF) was completed on a wavelength dispersive XRF S4 Pioneer system (Bruker AXS, Inc., Madison, WI). The powders were dispersed on a Chemplex polypropylene film of 12 μm thickness using an end window Rh X-ray tube with a 75 μm Be window for excitation in a helium atmosphere. Dynamic light scattering (DLS) on a Nanotrac ULTRA instrument (Microtrac, Inc., Montgomeryville, PA) was used to determine the particle size distribution of 0.01 g of powder dispersed in 25 mL of deionized water. The DLS samples were allowed to magnetically stir for 30 min and were ultrasonicated for 60 min before the measurements were taken. Each DLS measurement consisted of an average of five 30 s runs as is recommended by the instrument manufacturer and in conjunction with ASTM standard E2490−09. Surface area measurements were completed on a Micromeritics Tristar surface area and porosity analyzer (Micromeritics, Inc., Norcross, GA). The analysis was obtained using lightly ground powders with no other preparation procedures.

We also performed magnetic susceptibility measurements on the EuB_6 powders at different magnetic intensities from 2 K to room temperature using an MPMS-5 magnetometer (Quantum Design, San Diego, CA). In order to observe irreversible magnetic behavior, two measurement modes were used: zero-field cooling (ZFC) and field-cooling (FC). In ZFC the sample was first cooled to the minimum accessible temperature. Once in thermal equilibrium, the magnetic field was applied and the measurement was performed as the temperature was increased. The second mode, FC, was performed with the magnetic field applied by cooling the sample from room temperature to the minimum temperature.

3. RESULTS AND DISCUSSION

3.1. Boron Powders. The boron powders were tested for two main characteristics of possible importance during the chemical synthesis process: phase and morphology. Panels a and b in Figure 1 display the XRD patterns for the as-received B1 and B2 powders. The pattern for B1 was indexed to a $R\bar{3}m$ boron phase [PDF 00−011−0618] with lattice parameters of $a = 1.09520$ nm and $c = 2.38240$ nm, whereas the pattern for B2 was indexed to a different $R\bar{3}m$ boron phase [PDF 00−012−0377] with lattice parameters of $a = 0.409080$ nm and $c = 1.25670$ nm. This pattern contains four peaks that were not identifiable after an exhaustive analysis that included an unrestricted and thorough search in MDI JADE 9.0. Neither the B1 or B2 powders were amorphous, as reported by the vendor, although the B1 powders showed weak diffraction signal and broad peaks, indicative of some amorphous character. From the perspective of the phase of these two powders, both are very similar in crystalline character, thus, the phase differences in these precursor powders are expected to play a minor role in the chemical process during synthesis of the hexaborides. On the other hand, they have significantly different powder morphologies. (Figure 1c, d) illustrates the platelike (B1) and fiberlike (B2) morphologies between the two powders. The B1 powders have a surface area of 10.0 ± 0.1 m^2/g, whereas

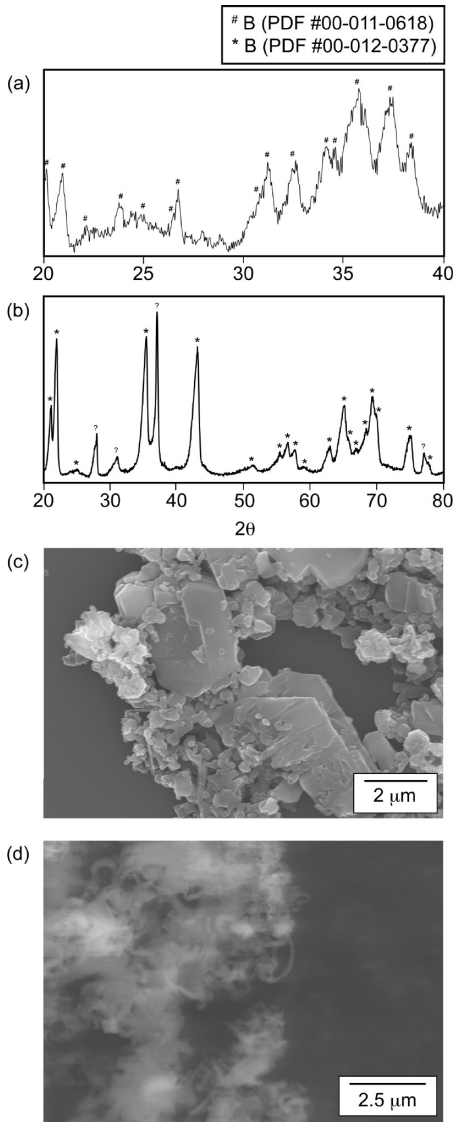

Figure 1. X-ray diffraction patterns and scanning electron micrographs of the as-received (a, c) B1 and (b, d) B2 powders.

the B2 powders have a surface area of 17.1 ± 0.1 m^2/g, as measured using BET analysis.

3.2. Synthesis and Characterization of Hexaboride Powders. Utilizing the B1 and B2 powders, the solution combustion process for the chemical synthesis of EuB_6, YbB_6, and YB_6, was analyzed. Sample names and a summary of XRD results are listed in Table I, where the "s" at the end of the name represents the as-synthesized powders and the "w" represents the washed powders. For the case of EuB_6 (PDF# 01−089−1411), the as-synthesized powders prepared using B1 [Eu−B1s] (Figure 2a) exhibit very minor impurity peaks of $EuBO_3$ (PDF 00−013−0485), whereas the as-synthesized powders prepared using B2 [Eu−B2s] (Figure 2b) show some level of amorphous character (centered at ∼30 and 45° 2θ). After acid cleaning, the powders have sharp EuB_6 peaks and a high level of crystallinity [Eu−B1w and Eu−B2w] (Figure 2c, d). The lattice parameter we obtained for these powders is 4.1839 Å, very close to the reported value of 4.19 Å.[13]

The synthesis of YbB_6 (PDF 03−065−1829) results in powders that have significant amounts of $YbBO_3$ (PDF 00−019−1427)

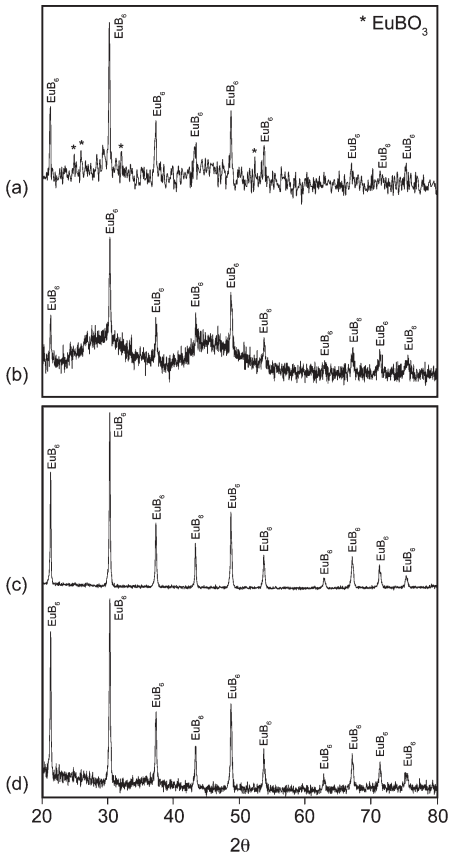

Figure 2. X-ray diffraction patterns of (a) Eu−B1s, (b) Eu−B2s, (c) Eu−B1w, and (d) Eu−B2w.

when prepared using both B1 and B2 [Yb−B1s and Yb−B2s] (Figure 3a, b). However, the powders prepared using B1 have the desired YbB_6 phase in higher amounts compared to powders prepared using B2, which only exhibit very minor amounts of YbB_6. After acid cleaning [Yb−B1w and Yb-b2w] (Figure 3c, d), the powders differ depending on which boron is used for synthesis. For the case of powders prepared using B1, the final powders contain mostly YbB_6 with some minor amounts of $YbBO_3$. The powders prepared using B2 consist only of $YbBO_3$. Finally, for the case of YB_6 (PDF 00−016−0732) synthesis, the as-synthesized powders prepared using B1 [Y−B1s] (Figure 4a), exhibit major peaks for YBO_3 (PDF 00−013−0531) and some diffraction signal from YB_6. The powders prepared using B2 [Y−B2s] (Figure 4b) only show peaks for YBO_3. Once acid cleaning is completed [Y−B1w and Y−B2w] (Figure 4c,d), the powders consist of mixed phases of YB_6, YB_{12} (PDF 00−013−0577), and YB_{25} (PDF 00−050−1493), which is not seen for the synthesis of EuB_6 or YbB_6. We propose that there is a dissolution and recrystallization process during acid cleaning, resulting in the mixed boride phases seen in the Y−B2w powders. This dissolution/recrystallization mechanism is evident for powders that remained in acid for long periods of time. In the particular example illustrated in Figure 5, the powders were in acid for 48 h, exemplifying the extreme situation of the dissolution/recrystallization process.

The success in obtaining EuB_6 by combustion synthesis can be explained by invoking differences in the ionic radii of Eu^{3+}, compared to the size of the unit cell, as well as differences in B−B bond distances. In hexaborides, the unit cell contains two types of

Table I. Listing of Prepared Samples and Resulting Phases in the As-Synthesized and Cleaned Powders

sample name	resulting phases
Eu−B1s	EuB_6 (major phase) $EuBO_3$ (minor phase)
Eu−B2s	EuB_6 (major phase) Amorphous material (minor phase)
Eu−B1w	EuB_6
Eu−B2w	EuB_6
Yb−B1s	$YbBO_3$, YbB_6 } approximately equal amounts
Yb−B2s	$YbBO_3$ (major phase) YbB_6 (minor phase)
Yb−B1w	YbB_6 (major phase) $YbBO_3$ (minor phase)
Yb−B2w	$YbBO_3$
Y−B1s	YBO_3 (major phase) YB_6 (minor phase)
Y−B2s	YBO_3
Y−B1w	YB_6, YB_{12}, YB_{25} } approximately equal amounts
Y−B2w	YB_6, YB_{12}, YB_{25} } approximately equal amounts

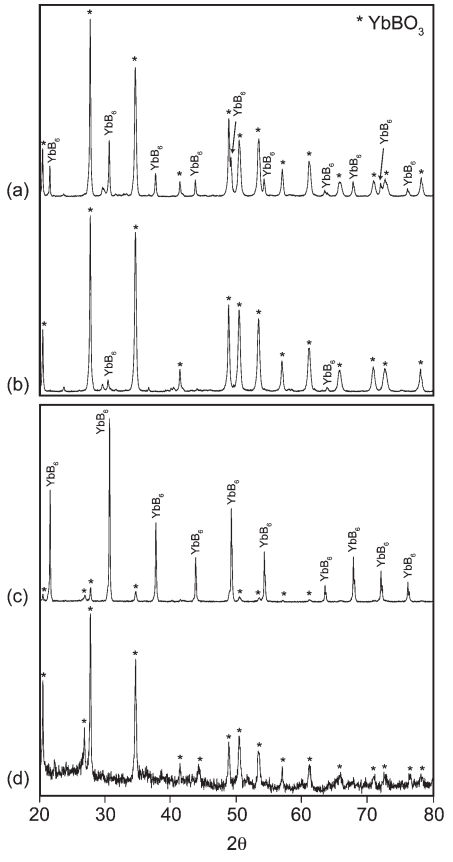

Figure 3. X-ray diffraction patterns of (a) Yb−B1s, (b) Yb−B2s, (c) Yb−B1w, and (d) Yb−B2w.

B−B bonds (Figure 6), one corresponding to the bond distances within the octahedral boron cages (i.e., intercage B−B bond distances), and the other corresponding to the bond distances between the boron cages (i.e., intracage B−B bond distances). As

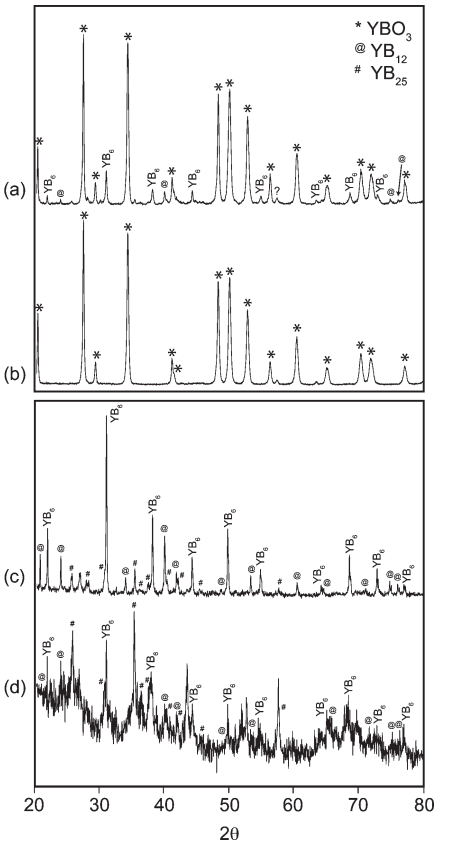

Figure 4. X-ray diffraction patterns of (a) Y−B1s, (b) Y−B2s, (c) Y−B1w, and (d) Y−B2w.

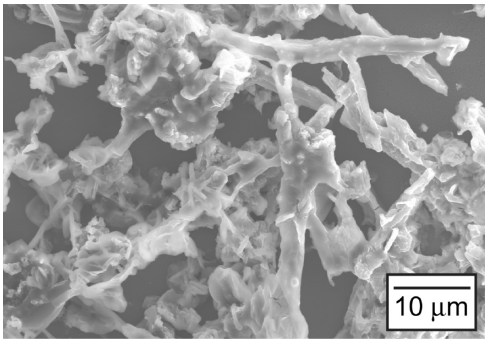

Figure 5. Scanning electron micrograph of EuB_6 powders that were left in acid for 48 h.

quantified in Figure 6a, the intercage distances are larger than the intracage distances for the case of hexaborides of Ca, Sr, Ba, La, Ce, Nd, Sm, and Eu. It is known that as the intracage distance increases, the strength of the bonds decreases, resulting in a decrease in compound stability.[14] Thus, hexaborides of Y, Gd, Tb, Dy, Ho, Er, Tm, Yb, and Lu are less stable compared to the former. Indeed, Ho and Lu do not form hexaborides, in support of this model.[15]

More importantly, variations in intracage B−B bond distances result in changes in the unit cell lattice parameters, which in turn changes the spacing inside the unit cell for the metal ions. With this in mind, Figure 6b quantifies the percent difference between the effective interstitial space, approximated as the body diagonal of a cube with edge dimension of [a − (Intracage B−B distance)],

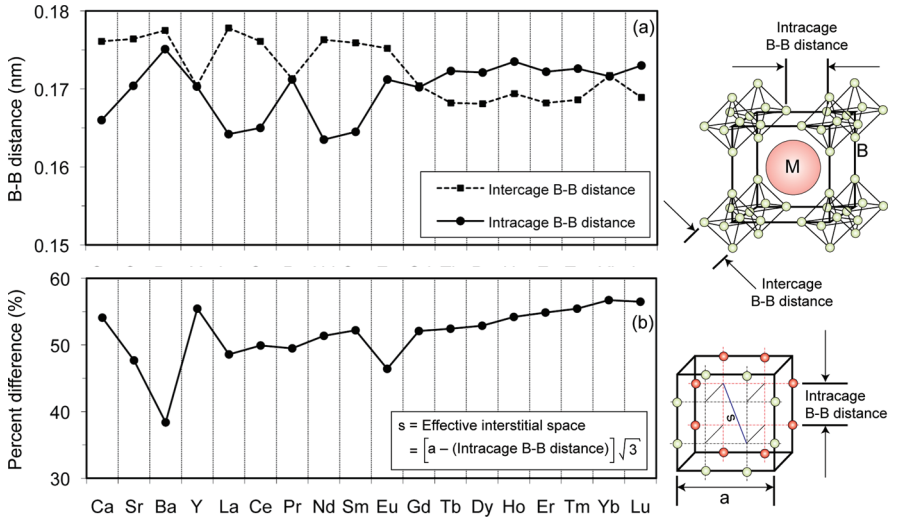

Figure 6. (a) Intracage and intercage B−B distances in hexaborides and (b) the percent difference between the interstitial space inside the hexaboride unit cell and the ionic radii of the metal ions in hexaborides.

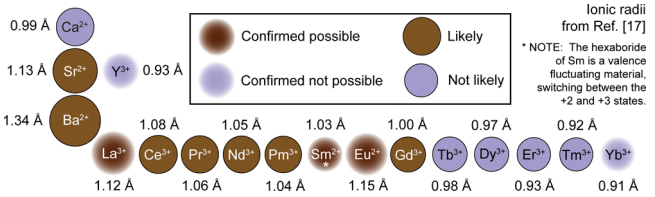

Figure 7. Prediction for formation of hexaborides based on the ionic radii of the metals. Ions with a radius larger than 1 Å can be effectively prepared by combustion synthesis.

and the diameter of the metal ions.[16] As can be seen, the difference between the interstitial space with respect to the ionic radius is largest for calcium, yttrium, and the rare-earth ions beyond terbium, with the difference increasing progressively with higher atomic number. Note that europium is particularly stable in this model, because of the difference between the interstitial space and the ionic radius is only 46.4%, similar to strontium (47.7%) and second lowest only to barium (38.4%). Gadolinium (52.09%) is at the edge of stability and could likely form by combustion synthesis. Calcium is an exceptional case in that the intracage distance is lower than the intercage distance, but the percent difference is still quite high, and thus, it is likely not a compound that can be formed by combustion synthesis.

From the above arguments, we propose that elements with cation radii that are small for the interstitial space in the center of the unit cell do not form hexaborides and, as the size increases, the hexaborides become progressively more stable. Because Yb^{3+} ($r_{Yb^{3+}}$ = 0.91 □) and Y^{3+} ($r_{Y^{3+}}$ = 0.93 □) are smaller than Eu^{2+} ($r_{Eu^{2+}}$ = 1.15 □), Sm^{3+} ($r_{Sm^{3+}}$ = 1.03 □), and La^{3+} ($r_{La^{3+}}$ = 1.12 □),[17] the formation of YbB_6 and YB_6 is difficult by combustion synthesis, because the process is extremely fast and completed in an air atmosphere, providing ready access to oxygen. Thus, it is not surprising that during the combustion reaction, the availability of oxygen results in the formation of $YbBO_3$ and YBO_3 compounds, at the expense of the hexaborides. As a general conclusion, illustrated in Figure 7 for all known metals that produce hexaborides, we maintain that hexaborides with a metal ion radius larger than approximately 1 Å, which results in an interstitial space that more effectively occupied, can be produced without difficulty by combustion synthesis. For the case of the rare-earth metals, any hexaboride to the left, and including, GdB_6 can be produced, whereas hexaborides to the right cannot be produced. The latter include TbB_6, DyB_6, ErB_6, TmB_6, and YbB_6.

We have also found that the morphology of the powders varies depending on which boron source is used during synthesis. The scanning electron microscope images in Figure 8 represent the as-synthesized and washed powders prepared using B1 and B2 for EuB_6 [Eu−B1w and Eu−B2w]. The powders obtained using B1 are significantly larger compared to the powders obtained using B2, both in the as-synthesized and cleaned states. For the cleaned powders prepared using B1, the particle size is centered around 630 nm, with a smaller distribution centered around 265 nm, whereas for the powders prepared using B2, the particle size is centered around 100 nm. The overall yield of the hexaboride phase from our process is currently 15−25%. This yield can be improved by optimizing the collection procedures used after each cleaning cycle and by performing the experiment in an oxygen-free environment. This would suppress formation of the borate phase, thereby increasing the yield of the hexaboride phase.

Our proposed mechanism for the solution combustion chemical synthesis process is illustrated in Figure 9. Starting with the platelike structure of the B1 powders, when the reactants are heated, the nitrates liquefy first forming a melt with boron powders dispersed in the melt. When the combustion reaction is initiated, the hexaboride material is formed on the surface of the boron particles, forming a discontinuous layer, followed by the formation of a borate layer on top of the hexaboride. When the powders undergo the initial hydrochloric acid wash, the borate phase at the top dissolves partially or fully, depending on how much is present in the powders. As a second step, the sulfuric acid penetrates the inside of the powder particles due to the discontinuous nature of the hexaboride covering, removing the unreacted boron and detaching the hexaboride powders from the surface of the boron particles. Further acid washing dissolves some of the hexaboride, forming cubes with low energy {100} surfaces (see Figure 8). The reaction mechanism for synthesis with B2 can be explained in a similar manner, but as the available surface area is high, entire particles convert to borate. resulting in

powders with much higher borate contents and quick dissolution of any phases present during acid washing, resulting in a smaller particle size. The presence of boron in the as-synthesized powders was determined by an EDS line scan across a sample of EuB_6 powders prepared using B1. As illustrated in Figure 10, as the scan proceeds from left to right, the center of a powder particle is traversed exhibiting an increased signal for boron and a decreased signal for europium, confirming the validity of our model.

Thus, it can be concluded that for hexaborides that can be obtained by combustion synthesis (i.e., LaB_6, SmB_6, EuB_6, and others with a metal ion radius larger than approximately 1 Å) the particle size of the boron is a defining parameter. In order to obtain hexaborides with a smaller particle size, the boron particle size should be as small as possible. In fact, the process can result in a variety of hexaboride particle sizes (large or small) based on

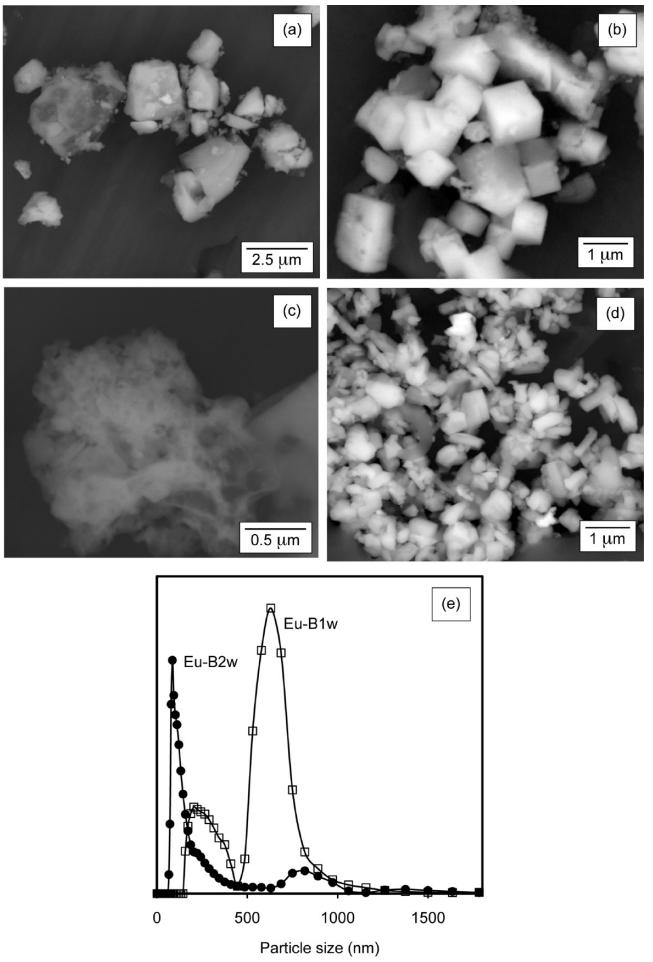

Figure 8. Scanning electron microscope images of (a) Eu−B1s, (b) Eu−B1w, (c) Eu−B2s, (b) Eu−B2w, and (e) particle size distribution from dynamic light scattering measurements.

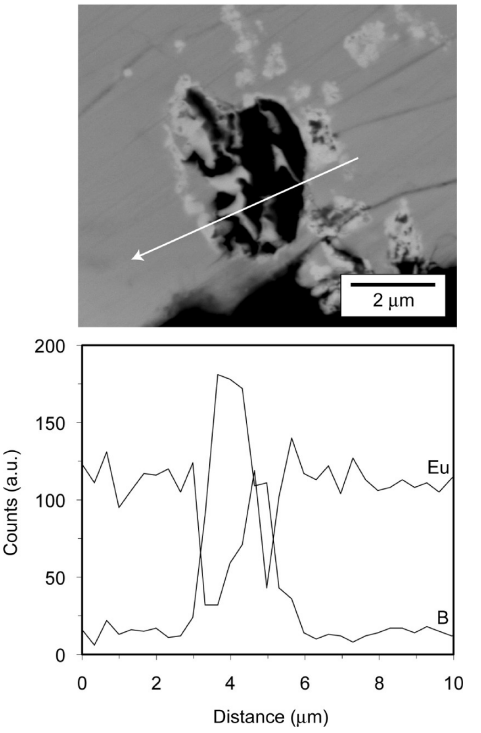

Figure 10. Energy-dispersive spectroscopy line scan across a Eu−B1s particle, showing an internal area of boron.

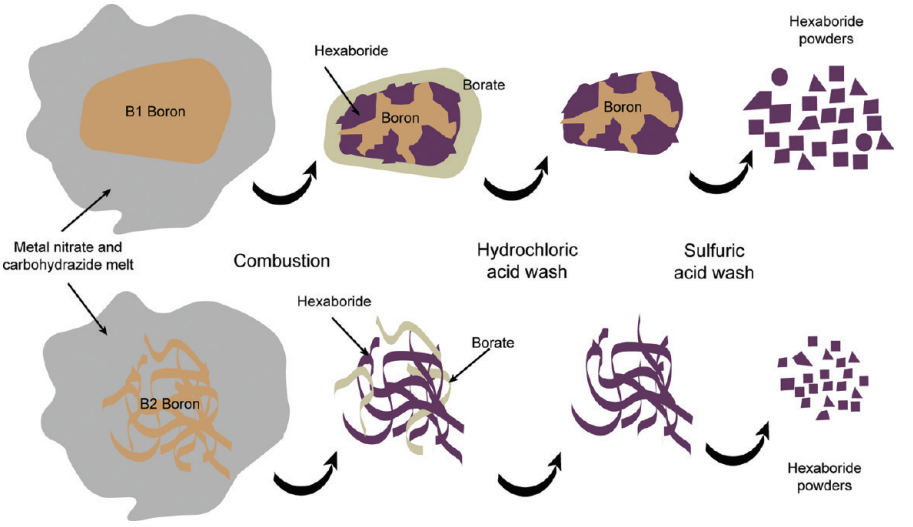

Figure 9. Mechanism of synthesis for the preparation of hexaborides by solution combustion synthesis.

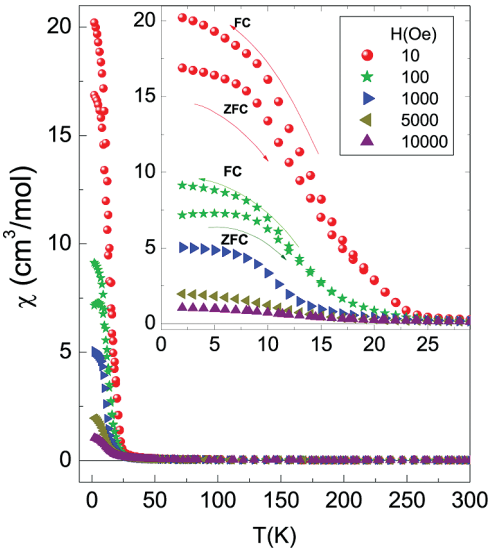

Figure 11. Magnetic susceptibility, χ, measured from 2 K to room temperature. The inset displays the low temperature region, where the ferromagnetic order is seen. We also note that the onset of ferromagnetism changes as the magnetic field intensity is changed.

variations in the boron particle size, a key advantage made possible by the combustion synthesis technique.

3.3. Magnetic Properties of EuB_6. Figure 11 illustrates the magnetic susceptibility, $\chi = M/H$, of the EuB_6 [Eu−B1w] powders. The susceptibility presents a steep increase at about 25 K. Above this temperature, the susceptibility displays a paramagnetic behavior, with χ close to zero, as expected for this compound.[6,8,18] The inset displays an amplification of the region from about 2 to 25 K, and measured with magnetic intensities from 10 to 10,000 Oe. In the low temperature region, $\chi(T)$ displays irreversible behavior at small magnetic intensities of 10 and 100 Oe, starting approximately at 12 and 17 K, respectively. On the other hand, measurements from 1000 to 10 000 Oe are reversible. As discussed earlier, Rhyee and Cho[9] have also found magnetic irreversibility for single crystals of $Eu_{0.9}La_{0.1}B_6$ at fields of 100 Oe and attributed it to the presence of the La dopant. Snow et al.[6] similarly have found that for La^{3+}-doped EuB_6 ($Eu_{1-y}La_yB_6$) single crystals, the magnetic susceptibility and the Curie temperature decrease with increasing amounts of La^{3+}. Their results show that small amounts of dopants ($y \leq 0.01$) have little effect on magnetic behavior, attributable to the highly local and pure-spin nature of the polarons. However, at $y \geq 0.03$ no magnetic polarons are present eliminating all magnetic response from the material.

Our own EuB_6 powders contain surface impurities that originate mostly from atmospheric exposure and possibly bulk impurities that originate from the reactants used during synthesis. XPS analysis of the EuB_6−B1 surfaces reveals an upper layer dominated by oxygen. The Eu 3d peaks (Figure 12a) at 1125 eV (Eu $3d_{5/2}$) and 1157 eV (Eu $3d_{3/2}$) agree with the data obtained in earlier reports[19−21] for the Eu^{2+} state, which is the ionic form present in EuB_6. The stronger Eu 3d peaks at 1135 and 1164 eV correspond to Eu^{3+}.[22] Vercaemst et al.[23] showed that Eu^{3+} is more stable than Eu^{2+} in the presence of oxygen. Accordingly, Eu is mostly found in a +3 state in the top layers of our powders. Some of the surface oxygen is in the form of hydroxide and can be seen from the binding energy peak at 532 eV for O 1s (Figure 12c).[24,25] From the B 1s signal (Figure 12b), we can surmise that the surface octahedral B_6 cages in the powders form a surface layer

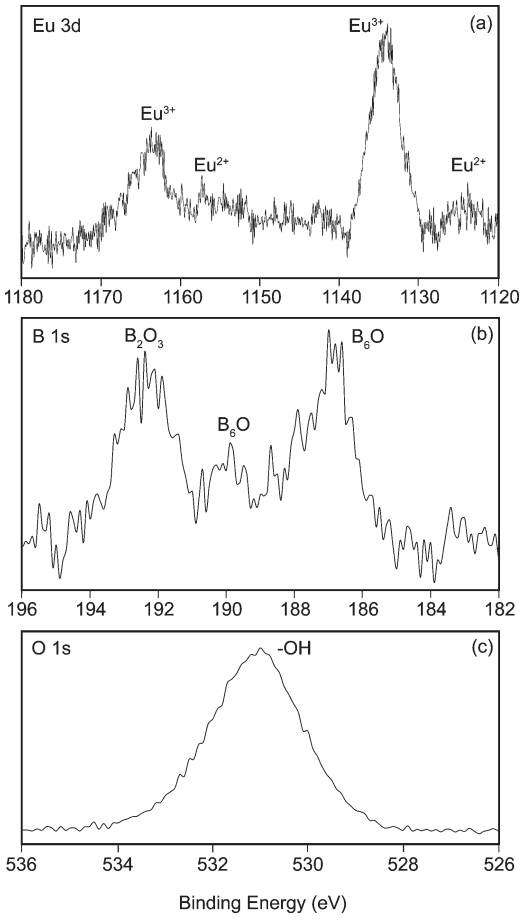

Figure 12. X-ray photoelectron spectra for Eu, B, and O in the Eu−B1s powders.

of B_6O with binding energy values of 187 and 189 eV.[26] In addition, the presence of B_2O_3 is detected from the peak at 193 eV.[27,28] The spectrum for O 1s does not show a signal for B−O in B_6O (located at 534 eV[26]) or Eu−O in Eu_2O_3 (located at 533 eV[27,29]) because those signals are located under the predominant O−H signal. From this analysis, we can conclude that the surface contains a layer of B_6O and Eu_2O_3, which are not magnetic.[30] Surface impurities that originate from the precursor chemicals are unlikely, because the powder surfaces are cleaned during the acid cleaning steps.

We also performed XRF analysis to determine if there were any significant bulk impurities. The only two signals detected from XRF were for europium and silicon. No other heavy elements were detected in the bulk powders. The presence of silicon is attributed to SiO_2 flakes that are independent of the EuB_6 particles. It is incorporated into the powders during synthesis from flaking of the Pyrex crystallization dishes and it is not seen in XRD because of its amorphous character. While low-atomic number elements are not detectable by XRF, we propose that these impurities, which could be incorporated into the bulk because of their presence in the precursor materials, are present in the powders only in small amounts. We infer this from the magnetic measurements. The presence of impurities in the amounts seen by Snow et al.[6] and Wigger et al.,[11] as required for modification of magnetic behavior, would be detected in XRD as either a lattice parameter change or possibly the formation of additional phases. This is clearly not evident from the XRD

results. We also know from the magnetic susceptibility measurements that our powders do not contain EuO, because this material would exhibit a response in magnetic susceptibility at approximately 69 K.[6] Accordingly, bulk impurities are not affecting the magnetic characteristics of our powders. We also believe that surface impurities are not responsible for this behavior, although we cannot completely rule them out. Surface effects might be particularly critical in our powders where the surface areas are high and surface impurities are significant. We postulate that surface effects are negligible because the magnetic susceptibility of the EuB_6 powders is extremely large and likely overwhelms any other signals from the surface.

The question remains regarding the cause for the irreversible behavior of the magnetic susceptibility at low fields and its disappearance at higher fields. We attribute this directly to the increase in size and number of magnetic polarons with increasing magnetic field, as was suggested by Snow et al.[6] for their doped EuB_6. Thus, we show that the effect of the coordinated behavior of the polarons is present in undoped EuB_6 powders and not just on doped single crystals. A more detailed analysis of this effect is currently underway.

In summary, two conditions have been found important for the successful combustion synthesis of phase-pure hexaboride powders: (1) powders can be obtained by combustion synthesis if the metal ion in the particular hexaboride has a radius greater than about 1 Å, and (2) the particle size of the hexaboride depends on the particle size of the precursor boron powders. In addition, we have shown that an increase in applied magnetic field results in an increase in size and number of magnetic polarons in EuB_6 powders.

4. CONCLUSIONS

The mechanisms of synthesis during solution combustion were determined for the preparation of hexaboride compounds. The three model systems analyzed in this study were EuB_6, YbB_6, and YB_6. The precursor materials for synthesis included appropriate metal nitrates, carbohydrazide as the combustion fuel, and two different boron powders of differing morphology and surface area. Results show that combustion synthesis is effective for the preparation of hexaborides when the metal ion has an ionic radius greater than approximately 1 Å. This includes EuB_6 and, from a previous study, LaB_6 and SmB_6. For compounds with a metal ion radius less than 1 Å, such as YbB_6 and YB_6, the synthesis process results in a significant amount of borate phase. The particle size of the EuB_6 product is dependent on the particle size of the precursor boron powders. This gives a level of control over the process that allows the fabrication of hexaboride powders of a variety of powder sizes. Magnetic measurements of the EuB_6 powders demonstrate that disruption of ferromagnetic polarons in the material can occur at low magnetic fields, as evidenced by the irreversible behavior seen in the magnetic susceptibility with respect to temperature. The magnetic response of the material can be attributed to an increase in size and number of magnetic polarons with increasing magnetic field.

AUTHOR INFORMATION

Corresponding Author

*E-mail: graeve@alfred.edu. Tel: (607) 871-2749. Fax: (607) 871-2354. URL: http://people.alfred.edu/~graeve/.

ACKNOWLEDGMENT

This project was funded by grants from the U.S. Army Research Office under Contracts W911NF-06-1-0226 and W911NF-08-1-0330. R.E. acknowledges support from UNAM-DGAPA Grant IN100711.

REFERENCES

(1) Cooper, S. L.; Nyhus, P.; Yoon, S.; Fisk, Z.; Sarrao, J. *Phys. B* **1998**, *244*, 133–137.
(2) Süllow, S.; Prasad, I.; Aronson, M. C.; Bogdanovich, S.; Sarrao, J. L.; Fisk, Z. *Phys. Rev. B* **2000**, *62*, 11626–11632.
(3) Brooks, M. L.; Lancaster, T.; Blundell, S. J.; Hayes, W.; Pratt, F. L.; Fisk, Z. *Phys. Rev. B* **2004**, *70*, 20401.
(4) Chatterjee, J.; Yu, U.; Min, B. I. *Phys. Rev. B* **2004**, *69*, 134423.
(5) Yu, U.; Chaterjee, J.; Min, B. I. *J. Appl. Phys.* **2005**, *97*, 10A903.
(6) Snow, C. S.; Cooper, S. L.; Young, D. P.; Fisk, Z.; Comment, A.; Ansermet, J.-P. *Phys. Rev. B* **2001**, *64*, 174412.
(7) Martinho, H.; Rettori, C.; Dalpian, G. M.; Da Silva, J. L. F.; Fisk, Z.; Oseroff, S. B. *J. Phys.: Condens. Matter* **2009**, *21*, 456007.
(8) Süllow, S.; Prasad, I.; Aronson, M. C.; Sarrao, J. L.; Fisk, Z.; Hristova, D.; Lacerda, A. H.; Hundley, M. F.; Vigliante, A.; Gibbs, D. *Phys. Rev. B* **1998**, *57*, 5860–5869.
(9) Rhyee, J.-S.; Cho, B. K. *J. Appl. Phys.* **2005**, *97*, 10A901.
(10) Yu, U.; Chaterjee, J.; Min, B. I. *J. Appl. Phys.* **2005**, *97*, 10A903.
(11) Wigger, G. A.; Beeli, C.; Felder, E.; Ott, H. R.; Bianchi, A. D.; Fisk, Z. *Phys. Rev. Lett.* **2004**, *93*, 147203.
(12) Kanakala, R.; Rojas-George, G.; Graeve, O. A. *J. Am. Ceram. Soc.* **2010**, *93*, 3136–3141.
(13) Tarascon, J. M.; Soubeyroux, J. L.; Etourneau, J.; Georges, R.; Coey, J. M. D.; Massenet, O. *Solid State Commun.* **1981**, *37*, 133–137.
(14) Etourneau, J.; Mercurio, J.-P.; Hagenmuller, P. In *Boron and Refractory Borides*; Matkovich, V. I., Ed.; Springer-Verlag: New York, 1977; pp 115−128.
(15) Etourneau, J.; Hagenmuller, P. *Philos. Mag. B* **1985**, *52*, 589–610.
(16) *ICSD Database Version 2010−2*; National Institute of Standards and Technology: Gaithersburg, MD, 2010.
(17) Dickinson, S. K. In *Ionic, Covalent, and Metallic Radii of the Chemical Elements*; AFCRL-70-0727 Physical Sciences Research Papers, No. 439; Air Force Cambridge Research Laboratories: Cambridge, MA, 1999.
(18) Geballe, T. H.; Matthias, B. T.; Andres, K.; Malta, J. P.; Cooper, A. S.; Corenzwit, E. *Science* **1968**, *160*, 1443–1444.
(19) Schneider, W. -D.; Laubschat, C.; Nowik, I.; Kaindl, G. *Phys. Rev. B* **1981**, *24*, 5422–5425.
(20) Pumera, M.; Cabala, M.; Veltruská, K.; Ichinose, I.; Tang, J. *Chem. Mater.* **2007**, *19*, 6513–6517.
(21) Mercier, F.; Alliot, C.; Bion, L.; Thromat, N.; Toulhoat, P. *J. Electron Spectrosc. Relat. Phenom.* **2006**, *150*, 21–26.
(22) Uwamino, Y.; Ishizuka, T.; Tamatera, H. *J. Electron Spectrosc. Relat. Phenom.* **1984**, *34*, 67–78.
(23) Vercaemst, R.; Poelman, D.; Fiermans, L.; Van Meirhaeghe, R. L.; Laflère, W. H.; Cardon, F. *J. Electron Spectrosc. Relat. Phenom.* **1995**, *74*, 45–56.
(24) Staib, Ph.; Dylla, H. F.; Rossnagel, S. M. *J. Vac. Sci. Technol.* **1980**, *17*, 291–3.
(25) Dupin, J. -C.; Gonbeau, D.; Vinatier, P.; Levasseur, A. *Phys. Chem. Chem. Phys.* **2000**, *2*, 1319–24.
(26) Belyansky, M; Trenary, M; Ellison, C. *Surf. Sci. Spectra.* **1995**, *3*, 147–150.
(27) Joyner, D. J.; Hercules, D. M. *J. Chem. Phys.* **1980**, *72*, 1095–1108.
(28) Burke, A. R.; Brown, C. R.; Bowling, W. C.; Glaub, J. E.; Kapsch, D.; Love, C. M.; Whitaker, R. B.; Moddeman, W. E. *Surf. Interface Anal.* **1988**, *11*, 353–358.
(29) Uwamino, Y.; Ishizuka, T.; Yamatera, H. *J. Electron Spectrosc.* **1984**, *34*, 67–78.
(30) Modak, S.; Acharya, S.; Bandyopadhyay, A.; Karan, S.; Roy, S. K.; Chakrabarti, P. K. *J. Magn. Magn. Mater.* **2010**, *322*, 283–289.